, COMMISSARIAT A L'ENERGIE ATOMIQUE

CENTRE D'ETUDES NUCLEAIRES DE SACLAY
Service de Documentation
F91191 GIF SUR YVETTE CEDEX

FR 9.10 1372

CEA-CONF-- 10441

P3

THERMOKINETIC MODEL OF BOROSILICATE GLASS DISSOLUTION; CONTEXTUAL AFFINITY

ADVOCAT T.- VERNAZ E.
CEA Centre d'Etudes Nucleaires de la Vallee du Rhone, 30 - Bagnols-sur-Ceze (FR)

CROVISIER J.L.- FRITZ B.
Centre National de la Recherche Scientifique, 67 - Strasbourg (FR)

Communication présentée à : 13. Symposium on the Scientific Basis for Nuclear Waste Management

Boston, MA (US)
27 Nov - 2 Dec 1989

THERMOKINETIC MODEL OF BOROSILICATE GLASS DISSOLUTION: CONTEXTUAL AFFINITY

T. ADVOCAT*, J.L. CROVISIER, B. FRITZ** and E. VERNAZ***
**CEN-Valrhô, SDHA, BP 171, 30205 Bagnols-sur-Cèze Cedex, France*
***CGS (CNRS), 1 rue Blessig, 67000 Strasbourg, France.*

ABSTRACT

Short and long-term geochemical interactions of R7T7 nuclear glass with water at 100°C were simulated with the DISSOL thermokinetic computer code. Both the dissolved glass quantity and the resulting water composition, saturation states and mineral quantities produced were calculated as a function of time. The rate equation used in the simulation was first proposed by Aagaard and Helgeson: $v = k^{+} \cdot S \cdot a(_{H^+})^{-n} \cdot (1 - e^{-(A/RT)})$. It simulates a gradually diminishing dissolution rate as the reaction affinity diminishes. The best agreement with 1-year experimental data was obtained with a reaction affinity calculated from silica activity (Grambow's hypothesis) rather than taking into account the activity of all the glass components as proposed by Jantzen and Plodinec. The concept of residual affinity was introduced by Grambow to express the fact that the glass dissolution rate does not cease. We prefer to replace the term "residual affinity" by "contextual affinity", which expresses the influence on the dissolution rate of three factors: the solution chemistry, the metastability of SiO_2(m), and the possible precipitation of certain aluminosilicates such as zeolites.

INTRODUCTION

The explicit expression of time in a predictive dissolution model requires the knowledge of an initial rate value and of a rate equation by which rate variations can be expressed as a function of extrinsic factors irrespective of the progress of the reaction.

A general rate equation was proposed by Aagaard and Helgeson[1], Helgeson *et al.*[2] and Lasaga[3] for hydrolysis of silicates, and was applied by Grambow[4] to nuclear glass dissolution. It requires a choice of activated complex (the desorption of which is a limiting factor) and knowledge of the pH and ion activity dependence.

The activity of the determining ions is used at each step of the reaction to define the *chemical affinity*: $A = RT \ln K/Q = -\Delta G_r(T,P)$ *in which* G_r *is the Gibbs free energy*, K *the* equilibrium constant, Q the ionic activity product, R the gas constant and T the temperature.

One of the main difficulties is to evaluate K for a glassy material, which we consider a turning point in kinetic modeling. A second difficulty is to define a realistic value for Q; in fact, Q is easily computed by standard geochemical codes, but is strongly dependent on the potential sequence of secondary products (e.g. code data bank), and on the equilibrium between solution and atmosphere (O_2 and CO_2 fugacity).

The purpose of this investigation was to study the influence of the choice of likely secondary products on the Q values, and its consequences on the reaction rate via the affinity. The DISSOL code can calculate a large composition field for clay minerals, one of the main secondary products in natural analogs, by a regular solid solution.

GENERAL CONSIDERATIONS

Short-Term Experimental Results

The glass dissolution mechanism was investigated experimentally at 90°C. The experimental procedure consisted in sampling fifteen 4 ml aliquots from each of two teflon leaching cells, which contained about 980 ml of stirred double-distilled water and monolithic glass specimens polished with silicon carbide powder to a final grain size of 4 μm; the experimental glass surface-area-to-solution-volume (SA/V) ratio was 10 m^{-1}. The relatively short time interval (10 to 140 hours)

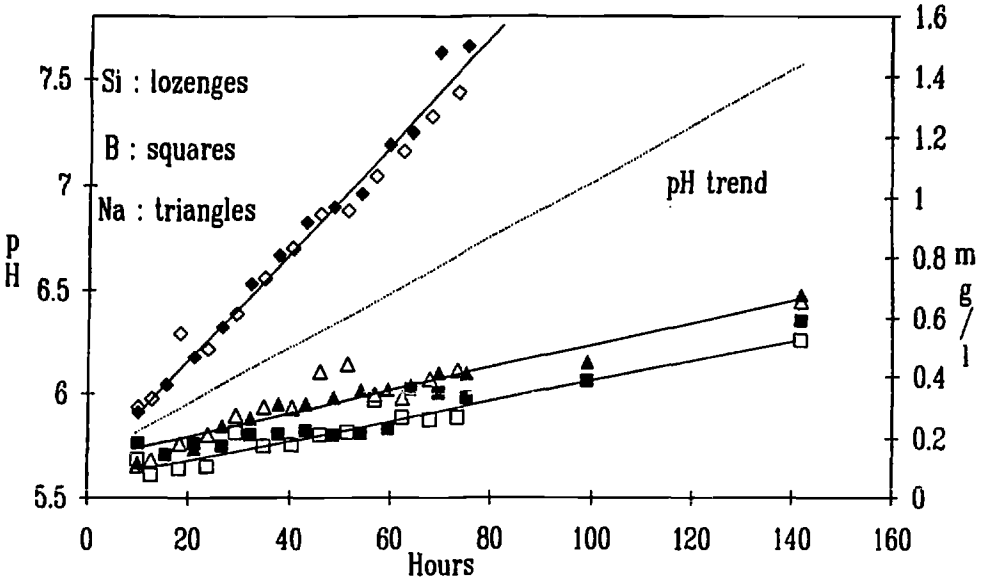

Figure 1a - Si, B and Na at 90°C and 10 m^{-1}: Regular samples from two leaching cells (solid symbols = cell 1; empty symbols = cell 2)

ensured that the initial reactant was far from saturation; this also prevented precipitation of silicates liable to affect a purely kinetic interpretation of the Si, B and Na concentrations in the solutions analyzed by ICP spectrometry. After 140 hours, the elemental concentrations did not exceed 2.8 mg·l^{-1} for Si, 0.59 mg·l^{-1} for B and 0.68 mg·l^{-1} for Na (Figure 1a). The pH at 90°C varied from 5.1 initially to 7.6 at the end of the experiment. Experimental repeatability was satisfactory, considering the slight dispersion of the analytical points around a linear evolution for virtually all the time intervals studied.

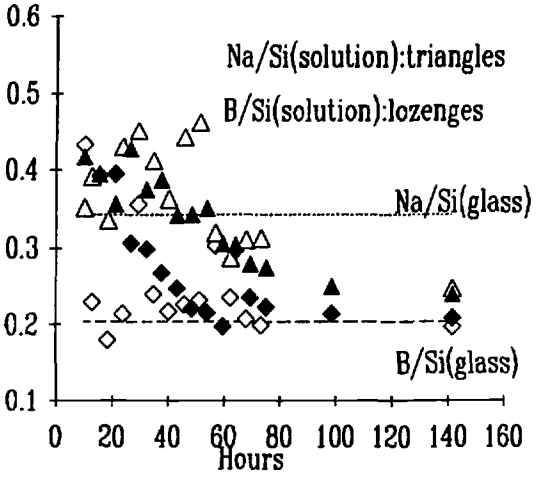

Figure 1b - Congruence ratios

The B/Si and Na/Si congruence ratios were indicative of initially selective dissolution lasting about 20 hours in one case and 40 hours in the other, followed by a stoichiometric dissolution phase. Beyond these intervals, the Na/Si and B/Si ratios tended towards 0.343 and 0.204, respectively, i.e. towards the corresponding ratios in R7T7 glass (Figure 1b): the medium was then neutral to slightly alkaline. Without surface analysis results, no explanation can currently be advanced for the evolution of the Na/Si ratio below the stoichiometric ratio after 60 hours. The dealkalinized glass thickness following initially selective dissolution was estimated at no more than 150 nm. The persistence of this preferential alkali metal corrosion front would indicate continued selective dissolution at this scale. However, this would not prevent dissolution of the residual siliceous structure, and extraction rates would be the same for glass network modifiers and network formers, corresponding to a globally congruent dissolution mechanism. The simulations described here take this mechanism into account.

The Concept of Residual Affinity

Experiments conducted under static conditions over a one-year period[5,6] showed that a higher SA/V ratio diminishes the glass dissolution rate; this was interpreted as the result of a gradual evolution towards saturation conditions in solution relative to the glass. Grambow[4] and Grambow and Strachan[7] introduced the concept of residual affinity to express the fact that long-term dissolution of a nuclear glass does not cease. This residual affinity was interpreted as an illustration of the properties of the silicated gel layer. This forces the silicon concentration (the impetus in dissolution kinetics[8]) to values slightly below saturation relative to the glass, resulting in a constant "residual" corrosion rate[4]. Experimental findings at very high SA/V ratios

(20 000 m^{-1}) published by Vernaz *et al.*[6] indicate that extremely low corrosion rates ($<2 \times 10^{-4}$ $g \cdot m^{-2} d^{-1}$) can be reached. We feel that long-term modeling cannot simply consist in extrapolating such an experimental rate. The formation of secondary phases of increasing stability cannot be disregarded as a potential controlling factor for the long-term dissolution rate[9]. Precipitation of analcime as observed by Van Iseghem *et al.*[10] increased the SAN 60 glass dissolution rate after one year. Similarly, Godon and Vernaz[11] demonstrated the effect of clay materials on the dissolution reaction affinity of R7T7 glass, and the persistence of high reaction rates for one year.

MODELING WITH DISSOL

Kinetic Dissolution Equation and Thermodynamic Calculations

Considerable experimental and theoretical work over the last decade on hydrolysis of silicated minerals has produced the following general kinetic relation:

$$v = k^{+} \cdot S \cdot a(_{H^+})^{-n} \cdot (1 - e^{-(A/RT)})$$

where $k^{+}_{(T,P)}$ is the kinetic constant; S the reactant/solution interface area; $a(_{H^+})$ the activity of species H^+ to which is assigned the stoichiometric reaction coefficient n corresponding to the reversible formation of the activated complex; R the ideal gas constant; T the temperature; and A the global reaction affinity. In the absence of experimental findings on the influence of the acidity of the aqueous medium on the initial dissolution rate at 100°C, the $k+ S a(_{H^+})^{-n}$ term is considered constant for these calculations.

The integral of the rate equation can be evaluated by first using the initial composition of the aqueous solution, assumed to be at homogeneous equilibrium during the reaction, and the molality and activity of all the aqueous species. These are calculated using the extended Debye-Hückel equation, by simultaneously solving the mass and charge conservation equations, and the mass action law representing the dissociation equilibria.

Aqueous phase saturation tests are then conducted as the reaction progresses. The result is the time-dependent relation of all changes in solution composition, and of the mass of reactant and products destroyed and formed.

Affinity Calculation for the Dissolution Reaction

Theoretically, as equilibrium conditions are approached, the reaction affinity diminishes: the ion activity product tends toward the reactant solubility product. Two hypotheses were considered. The first, based on the hydration concept formulated by Paul[12] and by Jantzen and Plodinec[13], assumes a global glass solubility as for minerals, calculated as the sum of the solubility products for the glass component oxides K_i with allowance for their mole fraction X_i (Table I):

$$\log K_{glass(100°C,1b)} = \sum_i (X_i \log K_i) + \sum_i (X_i \log X_i)$$

We added the mixture entropy term ($X_i \log X_i$) to account for the greater stability of an ideal solid solution relative to mechanical mixing. The second hypothesis, advanced by Grambow[4,5], only takes into account the activity of the aqueous species ($H_4SiO_4°$) in solution for the affinity calculation. The equilibrium value at 100°C for $\log K(SiO_2)_{glass}$ was set at −3.05; K was calculated from the experimental data reported by Fillet[14].

Initial Conditions and Modeling of Secondary Products

Various starting conditions were tested at 100°C. The pure water solutions were initially at atmospheric equilibrium ($pCO_2 = 10^{-3.5}$ atm corresponding to pH 5.9, and Eh = 350 mV). The gas pressures were held constant for one simulation, then varied during the next. Some elements in the R7T7 glass composition[14] were not taken into account (0.85% actinides and 11.24% fission products), but were simulated for calculation purposes by Li_2O, ZnO and MnO_2 (Table I). Alteration minerals tested include various carbonates, hydroxides, silicates and aluminosilicates such as zeolites, feldspars and phyllosilicates. The latter were simulated by an ideal solid solution model TOT "CISSFIT"[15,16] with the formula: $(Si_{4-x} Al_x)(Al, FeIII)O_{10}(OH)_2$ Na,Ca. The six pure end members contribute to the clay composition according to their degree of saturation

(Table I). This model was shown by Crovisier *et al.*[17] to reproduce the composition of clays and palagonite resulting from alteration of basaltic glasses. The initial dissolution rate of 4.9 $g \cdot m^{-2} d^{-1}$ was derived from work by Fillet[14] at 100°C with an SA/V ratio of 5 m^{-1}.

Results

Figure 2 shows the evolution of the concentrations for the major aqueous species in solution for both simulation tests. The initial calculation was based on a global glass reaction affinity at constant pCO_2 and pO_2. Under these conditions the calculated dissolution rate remained constant up to 2000 days, shown in Figure 2 by a virtually linear increase in the $B(OH)_3$ curve (broken line marked "GS"). The values for these elements were considerably overestimated in comparison with experimental results reported after 364 days by Fillet[14] (solid lozenges).

Another series of tests was conducted in which only $H_4SiO_4°$ was taken into account in the affinity calculation, as proposed by Grambow[4,5] and by Grambow and Strachan[7]. Under these conditions, DISSOL (solid lines in Figure 2) satisfactorily reproduced the silicon, boron and sodium concentrations measured by Fillet. At 364 days, for example, the calculated H_4SiO_4 concentration (i.e. the total silica content in solution) was 130 ppm, and the $B(OH)_3$ and Na^+ concentrations were 62 ppm and 17 ppm, respectively; the experimental values were 120 ppm, 75 ppm and 18 ppm, respectively.

The major events occurring during the simulation are indicated in Figure 2. The sequence of alteration products is characterized by early precipitation of iron hydroxide, then the TOT clay solid solution, followed by dissolution of $Fe(OH)_3$. Manganese hydroxide and then zinc hydroxide were precipitated before the transient formation of laumontite, a calcic zeolite. Calcium and strontium carbonates precipitated next, followed by metastable silica and albite. As soon as albite appeared, the laumontite totally dissolved. The first clay liable to form at 0.1 day was essentially calcic: $(Si_{3.05}Al_{0.95})(Fe_2)O_{10}(OH)_2(Ca_{0.47}Na_{0.01})$. At the end of the simulation (100 000 days) the clay composition was primarily sodic: $(Si_{3.01}Al_{0.99})(Fe_2)O_{10}(OH)_2Na_{0.98}$.

It is important to note that among the silicates tested, only the metastable compound $SiO_2(m)$ controls the $H_4SiO_4°$ concentration at a steady-state value below the glass saturation value. Without $SiO_2(m)$, DISSOL predicts a zero dissolution rate after one year. This is in disagreement with nuclear glass dissolution experiments in general, and with the results obtained by Fillet in particular. It was therefore necessary to include a pure siliceous compound in the model that constrained the $H_4SiO_4°$ concentration. Under these conditions, after 1086 days a sudden rise in the boron concentrations indicating renewed glass dissolution was observed as a result of two events:

- metastable SiO_2 precipitation maintained the $H_4SiO_4°$ concentration at a constant value,
- as the pH rose to strongly alkaline levels (>8.7) silicon was increasingly released into solution ($H_3SiO_4^-$ was the predominant aqueous species after 1086 days).

The secondary silicated products present in the greatest amounts over one year were laumontite, a transient mineral, and then the clay solid solution which gradually evolved toward sodic end members. Metastable silica and albite became the dominant silicated phases as soon as they were formed.

In another simulation, the saturation tests were extended to a wider range of zeolite compositions under identical initial conditions (previously only laumontite and analcime had been tested). Epistilbite, a calco-sodic zeolite (Table I) that precipitated at 1.2 day, delayed the drop in the dissolution rate over one year as observed experimentally by Fillet: the formation of this mineral implies consumption of a large fraction of the silicon released from the glass (Figure 3). The calculated concentrations (dotted lines marked "C") are well above the experimental values (symbols). For example, the calculated 364-day concentrations for H_4SiO_4, $B(OH)_3$ and Na^+ were 147 ppm, 91 ppm and 27 ppm, respectively, compared with the experimental values of 120 ppm, 75 ppm and 18 ppm. Note that the formation of this zeolite did not prevent a drop in the dissolution rate over one year.

The secondary mineralogical sequence of this simulation began with the transient formation of iron hydroxide at 0.008 day (not shown in Figure 3), followed by precipitation of the clay solid solution. Manganese and zinc hydroxides were formed next, followed by strontium carbonate and epistilbite, then by calcite and metastable silica. After about 2080 days, the precipitation of dachiardite, a more siliceous zeolite than epistilbite (cf Table I), destabilized the epistilbite and metastable silica, which then completely dissolved; the calculated H_4SiO_4, $B(OH)_3$ and Na^+ concentrations increased dramatically. Curve "C" (dotted lines in Figure 4) plots the kinetic equation relation $(1-(H_4SiO_4°)/(H_4SiO_4°)_{sat})$ versus time. The value sharply increases when

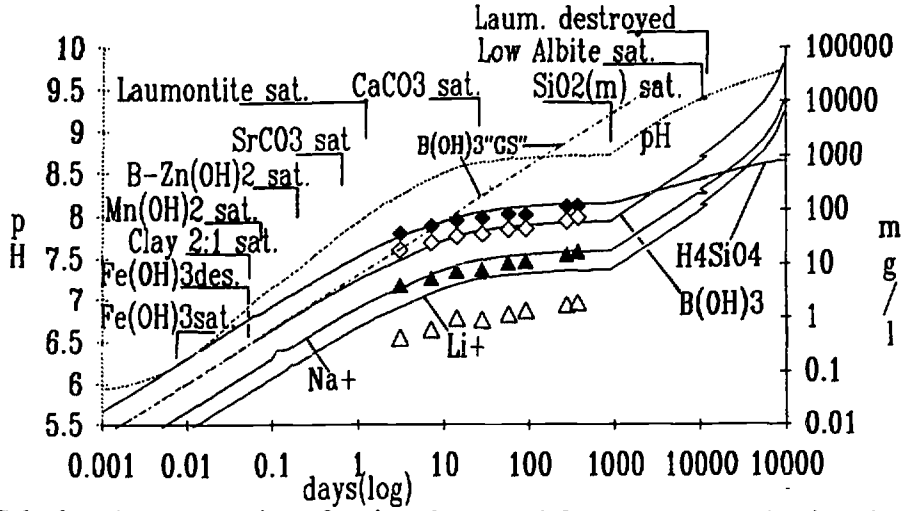

Figure 2 - Calculated concentration of major elements (100°C, constant pCO_2) and sequence of secondary products when reaction affinity is calculated using H_4SiO_4 (solid lines). "GS" refers to the global solubility hypothesis. Symbols represent experimental values reported by Fillet[14]: solid lozenges H_4SiO_4; empty lozenges $B(OH)_3$; solid triangle Na^+; empty triangle Li^+.

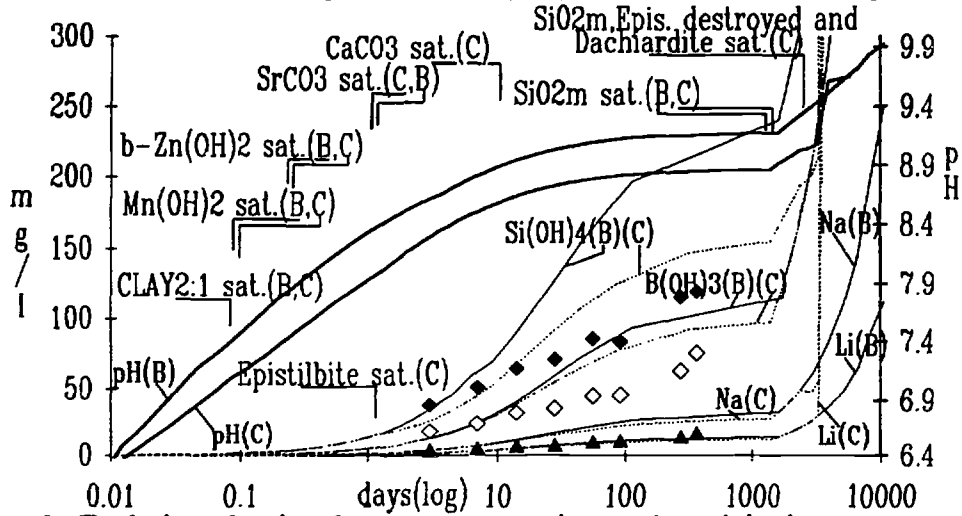

Figure 3 - Evolution of major element concentrations and precipitation sequences with various initial conditions: (B): variable pCO_2 and pO_2; (C): constant pCO_2 and pO_2 and all zeolites (Table I). Refer to Figure 2 for key to symbols.

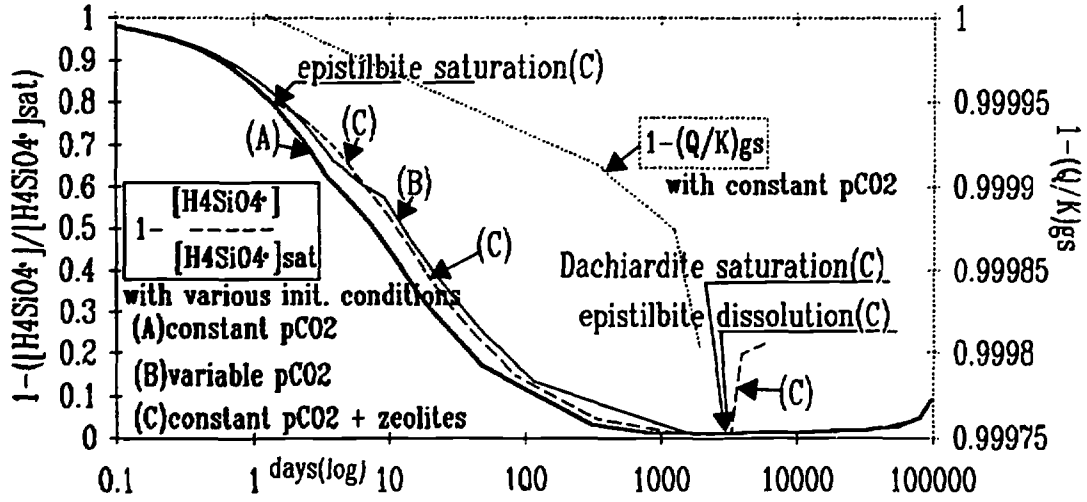

Figure 4 - Evolution of $(1-(H_4SiO_4°)/(H_4SiO_4°)_{sat})$ and (1-Q/K) term in kinetic relation versus time for different initial conditions tested with DISSOL at 100°C. The product of this expression by the initial rate (V_o) is equal to the instantaneous dissolution rate.

dachiardite is formed: the latter consumes not only epistilbite but also a significant fraction of the previously solubilized silica. The dissolution rate, i.e. the product of this expression and the initial (constant) rate, thus increases.

When simulations were conducted with variable CO_2 pressures (solid lines, Figure 3 "B") the carbonate buffer effect quickly became negligible, and the pH reached high values resulting in dissociation of the $H_4SiO_4°$ and a higher total silica concentration. The calculated values for total H_4SiO_4 then exceeded those measured by Fillet[14]: for example, the 364-day H_4SiO_4 and $B(OH)_3$ concentrations exceeded the measured results by 95 ppm and 20 ppm, respectively. Curve "B" (Figure 4) shows the effect of significant $H_4SiO_4°$ dissociation on the $(1-(H_4SiO_4°)/(H_4SiO_4°)_{sat})$ expression: the test values were higher than those obtained at constant pCO_2 (curve "A"), at least up to one year.

It is important to note that the long-term calculations were limited by the ionic strength of the solutions, which reached values above the range for which the Debye-Hückel law is valid. This was due to the unrenewed medium in which the calculations were performed, allowing the alkali metals and boron to accumulate passively in solution.

DISCUSSION

The results illustrate the importance of the hypotheses underlying the dissolution reaction affinity calculation. The assumption of a global affinity, for which all the elements in the glassy matrix are taken into consideration, does not account for the experimental results: this hypothesis (Figure 4) assumes that the initial rate persists for 2000 days, since the (1–Q/K) term does not drop below 0.998. An alternative hypothesis was advanced by Bourcier *et al.*[18] to account for the experimental results using the EQ3/EQ6 code. Bourcier suggests that the glass dissolution rate is determined by the decomposition rate of the reaction layer covering the glass surface (which does not contain any of the following compounds: B_2O_3, Na_2O, Li_2O, BaO).

Finally, Grambow's hypothesis, which considers only the $H_4SiO_4°$ for the affinity calculation, provided the best agreement with the experimental values. The existence of a "residual" rate as described by Grambow[4,5] and by Grambow and Strachan[7] can be explained by the nature of the siliceous gel that forms at the glass surface. In the simulations this was taken into account by a "metastable" form of SiO_2 (Table I) with an empirical solubility product below that of glass: precipitation of this compound prevents the dissolution rate from dropping to zero irrespective of the progress of the reaction. The higher the $SiO_2(m)$ solubility product in the gel (i.e. the higher the metastability), the lower the residual rate. Experiments at very high SA/V ratios[6] showed that this rate can drop to extremely low values, suggesting that the solubility product of $SiO_2(m)$ varies with the SA/V ratio. The essential question is whether a metastable compound can eventually evolve into a more stable form, in which case the glass dissolution rate would increase in time. Natural glass samples from Iceland studied by Crovisier *et al.*[17] showed that amorphous secondary phases can persist for more than 2.5 million years. However, the formation of certain zeolites predicted as potential phases could result in a significant long-term reduction in $H_4SiO_4°$ activity with a correlative increase in the glass dissolution rate[10].

The existence of a constant long-term residual affinity therefore cannot be demonstrated at the present time. The simulations showed that the long-term affinity depends on the geochemical context: Eh, pH, pCO_2, nature of secondary minerals and, above all, solubility of the siliceous compound $SiO_2(m)$. The calculations highlighted the critical role of certain zeolites, although they were not observed experimentally with R7T7 glass after one year at 100°C. This could be attributed to slow precipitation kinetics. The equations describing mineral precipitation kinetics are now being added to the DISSOL code to provide more accurate results. However, this requires currently unavailable experimental data (precipitation constants $k_{(T,P)}$, pH effects) and would not exclude the long-term consequences of their formation on the dissolution rate.

Long-term (10 000–100 000 year) modeling of glass behavior faces yet another difficulty: the alkali metals and boron tend to accumulate in solution rather than to become incorporated in mineral structures. This has two major consequences:

- The solution pH becomes strongly alkaline, leading to a reduction in the $H_4SiO_4°$ activity and, as suggested by curve "A" in Figure 4, a rise in the corrosion rate after 10 000 days, despite the constant difference between the solubility products of $SiO_2(m)$ and silica from the glass.
- The solution ionic strength rises well above 1, making it difficult to calculate the activities of the aqueous species with conventional activity coefficient functions.

Only long-term experiments at high SA/V values can show whether these calculations are realistic, or whether mineral phases not taken into consideration in the simulations can trap alkali metals in their structures.

CONCLUSION

Thermokinetic calculations in which a reaction affinity was computed with allowance only for the aqueous species $H_4SiO_4°$ were able to reproduce the overall one-year experimental variations reported by Fillet[14] and the major element concentrations to within an average of 10%. Most of the aluminosilicates predicted by the calculations have no effect on the glass dissolution rate, but the possible formation of a zeolite such as dachiardite could lead to a resumption of glass dissolution.

The hypothesis of a reaction affinity based exclusively on $H_4SiO_4°$ as suggested by Grambow and Strachan[7] requires allowance for a metastable polymorphous SiO_2(m) compound to account for the low experimental dissolution rates: its solubility product is then an empirical parameter of the model. The 1-year experimental dissolution rates diminish as the SA/V ratio rises, so the SiO_2(m) solubility limit cannot have a constant value. The nature of this polymorphous siliceous compound would therefore depend on the medium in which it is formed: the effect on the glass dissolution rate is the consequence of what we call "contextual affinity" rather than "residual affinity" which, according to our calculation, cannot be considered constant for long-term predictions. The principal difficulty now is to introduce the concept of variable stability of the SiO_2(m) component in long-term thermodynamic simulations. Without resolving this critical point, however, simulations of interactions between the backfill materials, the host rock and the glass should be performed using DISSOL. Repository media which could result in the formation of alteration products systematically more stable than SiO_2(m), i.e. controlling $H_4SiO_4°$ activity at values low enough to maintain significant dissolution rates, will always be more penalizing for glass than geological formations in which SiO_2(m) is formed.

REFERENCES

[1] P. Aagaard and H.C. Helgeson, Am. J. of Sci. 282, 237-285 (1982).
[2] H.C. Helgeson, W.M. Murphy and P. Aagaard, Geoch. Cosmoch. Acta, 48, 2405-2432 (1984).
[3] A.C. Lasaga, J. Geo. Res. 81B6, 4009-4025 (1984.
[4] B. Grambow, in *Scientific Basis for Nuclear Waste Management VIII*, (Mater. Res. Soc. Proc.) 44, 15-27 (1984).
[5] B. Grambow, SKB Technical Report 87-02 (1987).
[6] E. Vernaz, T. Advocat and J.L. Dussossoy, presented at the 4th International Symposium on Ceramics in Nuclear Waste Management (91st Am. Ceram. Soc. Meeting, 1989).
[7] B. Grambow and D.M. Strachan, in *Scientific Basis for Nuclear Waste Management XI*, (Mater. Res. Soc. Proc.) 112, 713-724 (1988).
[8] L.R. Pederson, C.Q. Buckwalter, G.L. McVay, R. Riddle, in *Scientific Basis for Nuclear Waste Management VI*, (Mater. Res. Soc. Proc.) 15, 47-54 (1982).
[9] R. Haaker, J. Malow and P. Offermann. in *Scientific Basis for Nuclear Waste Management VIII*, (Mater. Res. Soc. Proc.) 44, 121-128 (1985).
[10] P. Van Iseghem and B. Grambow, in *Scientific Basis for Nuclear Waste Management XI*, (Mater. Res. Soc. Proc.) 112, 631-639 (1988).
[11] N. Godon and E. Vernaz, in *Scientific Basis for Nuclear Waste Management* (this volume) (Mater. Res. Soc. Proc.).
[12] A. Paul, J. Mat. Sci., 12, 2246-2268 (1977).
[13] C.M. Jantzen and M.J. Plodinec, J. Non Cry. Sol., 67, 207-223 (1984).
[14] S. Fillet, PhD Thesis: University of Montpellier, France (1987).
[15] B. Fritz, Sci. Geol. Mem., 65, (1981).
[16] Y. Tardy and B. Fritz, Clays Minerals, 16, 361-373 (1981).
[17] J.L. Crovisier, T. Advocat, J.C. Petit and B. Fritz, in *Scientific Basis for Nuclear Waste Management XII*, (Mater. Res. Soc. Proc.) 127, 57-64 (1989).
[18] W.L. Bourcier, K.G. Knauss and C.I. Merzbacher, presented at 4th International Symposium on Ceramics in Nuclear Waste Management (91st Am. Ceram. Soc. Meeting, 1989).
[19] H.C. Helgeson, J.M. Delany, H.W. Nesbitt and D.K. Bird, Am. J. Sci, 274, 1089-1198 (1978).

Table I - Minerals Tested, Dissolution Equations
Sources: (1) Tardy and Fritz[16], Fritz[15]; (2) Crovisier *et al.*[17]; (3) Helgeson *et al.*[19]; (4) estimated from Vant Hoff equation and Paul[12]; (5) empirical value (see text).

GLASS	logK(100°C)	Molar Reaction Coefficient
Al_2O_3	-24.8	(3) 0.0296997
Na_2O	55.00	(3) 0.0981158
CaO	25.82	(3) 0.0444308
Fe_2O_3	-8.584	(3) 0.0112387
MnO_2	*(25°C) -28.04	(4) 0.0525288
SrO	41.39	(4) 0.0019642
Li_2O	*(25°C) 46.33	(4) 0.1409699
ZnO	8.54	(3) 0.0300151
B_2O_3	6.123	(4) 0.1242029
SiO_2	-2.201	(3) 0.4667340

SOLID SOLUTION END MEMBERS

Pyrophyllite	-36.761	(1)	$(Si_4Al_2O_{10}(OH)_2)+4H_2O<>4H_4SiO_4+2Al(OH)_4^-+2H^+$
Fe_3 Pyroph	9.347	(1)	$(Si_4Fe_2O_{10}(OH)_2)+6H^++4H_2O+2e^-<>4H_4SiO_4+2Fe^{2+}$
Ca-Muscovite	-40.09	(1)	$(Si_3Al_3O_{10}(OH)_2Ca_{0.5})+12H_2O<>3H_4SiO_4+3Al(OH)_4^-+0.5Ca^{2+}+2H^+$
Na-Muscovite	-40.592	(1)	$(Si_3Al_3O_{10}(OH)_2Na)+12H_2O<>3H_4SiO_4+3Al(OH)_4^-+Na^++2H^+$
Ca-FerriMusc	4.007	(1)	$(Si_3AlFe_2O_{10}(OH)_2Ca_{0.5})+6H^++4H_2O+2e^-<>3H_4SiO_4+Al(OH)_4^-+2Fe^{2+}+0.5Ca^{2+}$
Na-FerriMusc	3.505	(1)	$(Si_3AlFe_2O_{10}(OH)_2Na)+6H^++4H_2O+2e^-<>3H_4SiO_4+Al(OH)_4^-+2Fe^{2+}+Na^+$

OTHER MINERALS TESTED

Gibbsite	-12.17	(3)	$Al(OH)_3+H_2O<>Al(OH)_4^-+H^+$
Amorph. iron	13.9	(3)	$Fe(OH)_3+3H^++e^-<>Fe^{2+}+3H_2O$
SiO_2(m)	-3.055	(5)	$SiO_2+2H_2O<>H_4SiO_4$
Portlandite	18.15	(3)	$Ca(OH)_2+2H+<>Ca^{2+}+2H_2O$
B-$Zn(OH)_2$	8.77	(4)	$Zn(OH)_2+2H+<>Zn^{2+}+2H_2O$
Boehmite	-12.156	(3)	$AlO(OH)+2H_2O+<>Al(OH)_4-+H+$
$Mn(OH)_2$	8.41	(4)	$Mn(OH)_2+2H+<>Mn^{2+}+2H_2O$
Petalite	-3.21	(4)	$(LiAlSi_4O_{10})+10H_2O<>Al(OH)_4^-+Li^++4H_4SiO_4$
Halloysite	-28.75	(3)	$(Si_2Al_2O_5(OH)_4)+7H_2O<>2Al(OH)_4^-+2H_4SiO_4+2H^+$
Calcite	-9.39	(3)	$CaCO_3<>Ca^{2+}+(CO_3)^{2-}$
Rhodocrosite	-11.56	(3)	$MnCO_3<>Mn^{2+}+(CO_3)^{2-}$
Smithsonite	-10.88	(4)	$ZnCO_3<>Zn^{2+}+(CO_3)^{2-}$
Strontianite	-11.69	(3)	$SrCO_3<>Sr^{2+}+(CO_3)^{2-}$
Low Albite	-16.037	(3)	$(NaAlSi_3O_8)+8H_2O<>Al(OH)_4^-+Na^++3H_4SiO_4$
Anorthite	-17.26	(3)	$(CaAl_2Si_2O_8)+8H_2O<>2Al(OH)_4^-+Ca^{2+}+2H_4SiO_4$
Nepheline	-7.41	(3)	$(NaAlSiO_4)+4H_2O<>Al(OH)_4^-+Na^++H_4SiO_4$
Analcite	-11.19	(3)	$(NaAlSi_2O_6\cdot H_2O)+5H_2O<>Al(OH)_4^-+Na^++2H_4SiO_4$
Laumontite	-27.38	(3)	$(CaAl_2Si_4O_{12}\cdot 2H_2O)+10H_2O<>2Al(OH)_4^-+Ca^{2+}+4H_4SiO_4$
Na-Chabazite	-54.6	(2)	$(Na_{3.5}Ca_{0.25}Al_4Si_8O_{24}\cdot 13H_2O)+11H_2O<>4Al(OH)_4^-+3.5Na^++0.25Ca^{2+}+8H_4SiO_4$
Ca-Chabazite	-57.64	(2)	$(Ca_2Al_4Si_8O_{24}\cdot 13H_2O)+11H_2O<>4Al(OH)_4^-+2Ca^{2+}+8H_4SiO_4$
Epistilbite	-55.56	(2)	$(Ca_{1.5}Al_3Si_9O_{24}\cdot 8H_2O)+16H_2O<>3Al(OH)_4^-+1.5Ca^{2+}+9H_4SiO_4$
Heulandite	-40.07	(2)	$(Ca_{0.9}Na_{0.2}Al_2Si_7O_{18}\cdot 6H_2O)+12H_2O<>2Al(OH)_4^-+0.2Na^++0.9Ca^{2+}+7H_4SiO_4$
Dachiardite	-105.16	(2)	$(Na_{2.5}Ca_{1.25}Al_5Si_{19}O_{48}\cdot 12H_2O)+36H_2O<>5Al(OH)_4^-+2.5Na^++1.25Ca^{2+}+19H_4SiO_4$
Mordenite	-49.4	(2)	$(Al_2NaCa_{0.5}Si_{10}O_{24}\cdot 6H_2O)+18H_2O<>2Al(OH)_4^-+Na^++0.5Ca^{2+}+10H_4SiO_4$
Ca-Gmelinite	-29.18	(2)	$(CaAl_2Si_4O_{12}\cdot 6H_2O)+6H_2O<>2Al(OH)_4^-+Ca^{2+}+4H_4SiO_4$
Na-Gmelinite	-27.46	(2)	$(Na_2Al_2Si_4O_{12}\cdot 6H_2O)+6H_2O<>2Al(OH)_4^-+2Na^{2+}+4H_4SiO_4$
Na-Clinoptilol	-48.30	(2)	$(Al_2Na_{1.8}Ca_{0.1}Si_{10}O_{24}\cdot 8H_2O)+16H_2O<>2Al(OH)_4^-+1.8Na^++0.1Ca^{2+}+10H_4SiO_4$